

# Application of Neural Networks for Estimating Coseismic Slip Distribution Using Synthetic GNSS Data

V. Inzunza \*<sup>1</sup>, M. Moreno <sup>2</sup>, V. Yáñez-Cuadra <sup>3</sup>, F. Ortega-Culaciati <sup>4,5</sup>, I. Calisto <sup>1</sup>, M. Miller <sup>1</sup>

<sup>1</sup>Departamento de Geofísica, Universidad de Concepción, Víctor Lamas 1290, Concepción, 4030000, Chile, <sup>2</sup>Departamento de Ingeniería Estructural y Geotécnica, Pontificia Universidad Católica, Santiago, Chile, <sup>3</sup>TerraSur Geofísica, Concepción, Chile, <sup>4</sup>Departamento de Geofísica, Facultad de Ciencias Físicas y Matemáticas, Universidad de Chile, Santiago, Chile, <sup>5</sup>Data Observatory Foundation, ANID Technology Center No DO210001, Santiago, Chile

**Author contributions:** *Conceptualization:* V. Inzunza, M. Moreno, V. Yáñez-Cuadra, F. Ortega-Culaciati, I. Calisto. *Methodology:* V. Inzunza, V. Yáñez-Cuadra, F. Ortega-Culaciati. *Software:* V. Inzunza, V. Yáñez-Cuadra. *Formal Analysis:* V. Inzunza, M. Moreno. *Data Curation:* M. Moreno. *Writing - Original draft:* V. Inzunza, M. Moreno, V. Yáñez-Cuadra, F. Ortega-Culaciati. *Writing - Review & Editing:* I. Calisto, M. Miller. *Supervision:* M. Moreno.

**Abstract** Accurately and rapidly estimating coseismic slip is crucial for characterizing the rupture and magnitude of earthquakes and improving early warning systems. However, slip inversions often involve hyperparameters related to prior information, whose selection significantly affects solution efficiency and quality. In this study, we present a novel method for estimating fault slip distributions from GNSS displacements using neural networks. The method was initially developed with synthetic models to define an optimal architecture for accurately recovering target slip. This approach demonstrated exceptional computational efficiency, delivering accurate slip distribution predictions in just 0.07 seconds without specialized hardware. The method was then validated with real-world data from the 2015  $M_w$  8.3 Illapel earthquake, achieving a GNSS displacement RMSE of 0.07 m and yielding a slip distribution consistent with published solutions. Compared to Regularized Least Squares (RLS) inversion, the neural network estimated slip closer to the trench, aligning with tsunami observations despite slightly higher residuals. Additionally, hyperparameter exploration revealed that using the GELU activation function and a 35% dropout rate provided the best balance. Model performance improved with larger datasets, and while reducing GNSS stations increased uncertainty, more data enhanced accuracy. These findings highlight the importance of hyperparameter tuning and data selection in improving slip estimations, offering insights for future improvements.

Production Editor:  
Andrea Llenos  
Handling Editor:  
Wenbin Xu  
Copy & Layout Editor:  
Hannah F. Mark

Received:  
November 22, 2024  
Accepted:  
April 8, 2025  
Published:  
May 19, 2025

## 1 Introduction

Plate tectonics, through the accumulation and release of strain, is responsible for the most powerful earthquakes on Earth, especially within subduction zones, where one tectonic plate slides under another. Subduction zones have the potential to produce devastating tsunamigenic earthquakes, such as the 2004  $M_w$  9.1 Sumatra-Andaman earthquake (e.g., Okal and Stein, 2009; Lay et al., 2005; Chlieh et al., 2007) and the 2011  $M_w$  9.0 Tohoku earthquake (e.g., Fujii et al., 2011; Ozawa et al., 2012; Tajima et al., 2013; Simons et al., 2011). In these convergent margins, elastic strain energy builds up over decades or centuries, with a significant fraction being subsequently released during earthquakes within the shallow part of the subduction interface. Chile is a highly active seismic region (e.g., Cisternas et al., 2017), where some of the largest-magnitude earthquakes ever recorded have occurred along the subduction zone where the Nazca Plate subducts beneath the South American Plate at a rate of 66 mm/year (Altamimi et al., 2016). Notable recent events at this margin include the 1960  $M_w$  9.5 Valdivia Earthquake (e.g., Barrientos and Ward, 1990; Fujii and Satake, 2012; Lorenzo-

Martín et al., 2006), the 2010  $M_w$  8.8 Maule Earthquake (e.g., Moreno et al., 2010, 2012; Bedford et al., 2013; Delouis et al., 2010), the 2014  $M_w$  8.2 Iquique Earthquake (e.g., Duputel et al., 2015; Jara et al., 2018; Meng et al., 2015) and the 2015  $M_w$  8.3 Illapel Earthquake (e.g., Melgar et al., 2016; Tilmann et al., 2016; Heidarzadeh et al., 2016).

Within the past few decades, the use of Global Navigation Satellite System (GNSS) stations has significantly improved the observation of both interseismic and coseismic surface displacements, advancing our understanding of earthquake dynamics. As GNSS stations have become more widespread globally, they now provide high-resolution measurements of crustal deformation, especially in subduction zones, allowing us to identify the characteristics and behaviors of large megathrust earthquakes (e.g., Ruegg et al., 2009; Chen et al., 2015; Luo et al., 2020). Estimating coseismic slip of earthquakes is essential to comprehending the underlying mechanics, including energy release, stress redistribution, and fault dynamics. This understanding is vital for seismic risk evaluation, developing mitigation strategies, and informing rapid response efforts (Iinuma et al., 2012).

\*Corresponding author: valentina.inz.gar@gmail.com

involve constructing a linear forward model through the generation of Green's functions based on elastic dislocations (e.g., Okada, 1985; Nikkhoo and Walter, 2015). Despite the linearity of the forward model, estimating coseismic slip remains a complex and ill-posed inverse problem, characterized by non-unique solutions. There are two end-member approaches to deal with the inverse problem. The first, known as the optimization approach, focuses on finding a solution to the inverse problem that minimizes a data misfit term and a regularization term, the latter used to define prior information that stabilizes the solution (e.g., Harris and Segall, 1987; Ortega-Culaciati et al., 2021). The second is a Bayesian approach, where an ensemble of models is sampled from a posterior probability distribution of slip (e.g., Minson et al., 2013; Duputel et al., 2014).

With the advance of technology and the proliferation of big data, Machine Learning (ML) algorithms have taken on a significant role in seismological problems. Recent progress includes the application of deep learning techniques for detecting low-frequency earthquakes (Münchmeyer et al., 2024) and denoising HR-GNSS data (Thomas et al., 2023), as well as the automatic identification of slow slip events (Donoso et al., 2021), tectonic analysis through the clustering of interseismic velocities from GNSS stations (e.g., Yañez-Cuadra et al., 2023), earthquake magnitude estimation (Lin et al., 2021), coseismic slip distribution prediction (Cui et al., 2024), and estimation of plate interface locking using supervised ML (Barra et al., 2024).

In this study, we propose a novel and efficient approach to estimate coseismic slip by employing artificial neural networks, where we define prior information on slip through the characteristics of the training set — in a similar manner as Barra et al. (2024) — to improve stability and deal with the complexities of the ill-posed inverse problem. Our model is trained using a diverse set of synthetic earthquake scenarios, designed to reflect a wide range of fault slip behaviors.

Unlike traditional inversion methods, which require explicit regularization and can be computationally expensive, our approach implicitly incorporates prior constraints through the characteristics of the training dataset—similar to Barra et al. (2024)—enhancing solution stability and addressing the ill-posed nature of the inverse problem. Our model consists of a neural network trained to infer the slip distribution from surface GNSS displacements. To achieve this, we generate a diverse set of synthetic earthquake scenarios ensuring that the training data captures a wide range of slip behaviors. By learning the relationship between surface deformation and fault slip, the neural network provides a fast and data-driven alternative to conventional inversion techniques. Once trained, the neural network uses GNSS observations to predict coseismic slip.

Once the model is trained, we evaluate its effectiveness in a real-world scenario by estimating the coseismic slip of the September 16, 2015 ( $M_w$  8.3) Illapel, Chile, earthquake. Widely felt across the region, this earthquake shook a broad segment of the central Chilean subduction zone at 22:54:31 (UTC). We constrained the slip distribution using GNSS co-seismic dis-

placements available from Klein et al. (2017). Furthermore, we conduct a sensitivity analysis on different hyperparameters and data conditions that impact the performance of the neural network. This analysis is crucial for demonstrating the sensitivity of our model to different settings and optimizing its configurations. To validate our methodology, we compare it with the traditional Regularized Least Squares inversion technique to identify and evaluate the differences in performance between these two methods.

## 2 Methods

### 2.1 Synthetic Earthquake Data

We used the SLAB 2.0 geometry defined by Hayes et al. (2018) to represent the subduction megathrust fault interface. This geometry is discretized into a triangular mesh consisting of 1002 elements across Cartesian coordinates ranging from approximately 29°S to 33°S along the Chilean coastline, corresponding to the area impacted by the Illapel earthquake. Green's functions, for modeling the surface displacements due to subsurface slip, are derived using the *TDispHS* triangular dislocation model by Nikkhoo and Walter (2015).

For the generation of synthetic earthquakes, we adapted the code developed by Carr Agnew (2013), originally designed to simulate synthetic GNSS time series for slow slip events, to incorporate a representation of surface displacements associated with slip distributions of synthetic earthquakes. For simulating coseismic slip, we employed a linear forward model to relate coseismic slip on the fault interface, along both the strike and dip components, to the GNSS surface displacements. The synthetic dataset was generated at the positions of the 107 continuous GNSS stations provided by Klein et al. (2017), which include continuous (daily) and survey data.

Synthetic earthquake slip distributions are modeled as elliptical sources, each generated by sampling source parameters from uniform distributions. The ellipse dimensions are set within specific ranges, while slip magnitudes are assigned within predefined limits. Rake angles are based on typical values observed in Chilean seismic subduction events, and Gaussian noise is added to the calculated surface displacements to reflect the standard deviation of the uncertainties reported for the GNSS stations. These synthetic earthquakes, with magnitudes ranging from approximately  $M_w$  7 to  $M_w$  9, have spatial extents that fall within the mesh dimensions. The ranges used for the properties of these synthetic earthquake sources are detailed in Table 1. An overview of the geometry, GNSS station distribution, and examples of synthetic slip scenarios is shown in Figure 1.

Properties	Minimum	Maximum
Slip (m)	5	20
Rake (°)	80	100
Length (km)	30	300

**Table 1** Properties of synthetic earthquake slips and ellipses: This table summarizes the minimum and maximum values for slip magnitude, rake angle, and length extent.

After training our model, we employed Monte Carlo error propagation to estimate uncertainties arising from measurement errors, which were assumed to follow independent Gaussian distributions with standard deviations based on actual measurements. To assess these uncertainties, we generated 50,000 data realizations, a slightly larger number than that used by [Barra et al. \(2024\)](#).

## 2.2 Least Squares Inversion

For the quasi-static slip estimation problem, the relationship between observed data ( $\mathbf{d}$ ) and model parameters ( $\mathbf{m}$ ) is often represented as the linear forward model:

$$\mathbf{d} = \mathbf{G}\mathbf{m} \quad (1)$$

where the Green's function matrix  $\mathbf{G}$  defines a mapping from model parameters  $\mathbf{m}$  into observable data  $\mathbf{d}$  vector spaces, thus allowing us to predict the data for a particular model  $\mathbf{m}$ . The inverse problem deals with the estimation of values of  $\mathbf{m}$ , given experimental observations  $\mathbf{d}$  and their relation defined by the forward model (e.g., [Menke, 1989](#); [Tarantola, 2005](#); [Aster et al., 2013](#)).

Among the various inversion techniques that can be applied to estimate a slip distribution, the Least Squares method is widely utilized due to its simplicity and ease of uncertainty quantification, as it has an analytical solution for the estimated model and the covariance matrix representing its uncertainties. This method aims to find the model parameters  $\mathbf{m}$  that minimize the sum of the squared differences between the observed data and their prediction by the forward model ([Lawson and Hanson, 1995](#)).

As slip inversion is known to be a highly ill-posed problem, a regularization term is often added to the objective function of the Least Squares problem. In most cases, slip inversion relies in solving the Least Squares problem with Tikhonov Regularization,

$$\min_{\mathbf{m}} \|\mathbf{W}_d(\mathbf{G}\mathbf{m} - \mathbf{d})\|_2^2 + \varepsilon^2 \|\mathbf{H}\mathbf{m}\|_2^2 \quad (2)$$

where  $\mathbf{W}_d$  is a weight matrix such that  $\mathbf{W}_d^T \mathbf{W}_d = \mathbf{C}_d^{-1}$ ,  $\mathbf{C}_d$  is the covariance matrix of the observed data  $\mathbf{d}$ ,  $\mathbf{H}$  is a regularization operator, and  $\varepsilon$  is a regularization parameter that needs to be determined using a model class selection technique (e.g., [Craven and Wahba, 1978](#); [Hansen and O'Leary, 1993](#)). The solution of equation 2 can be written as,

$$\tilde{\mathbf{m}} = (\mathbf{G}^T \mathbf{C}_d^{-1} \mathbf{G} + \varepsilon^2 \mathbf{H}^T \mathbf{H})^{-1} \mathbf{G}^T \mathbf{C}_d^{-1} \mathbf{d} \quad (3)$$

$$\widetilde{\mathbf{C}}_m = (\mathbf{G}^T \mathbf{C}_d^{-1} \mathbf{G} + \varepsilon^2 \mathbf{H}^T \mathbf{H})^{-1} \quad (4)$$

where  $\tilde{\mathbf{m}}$  is the estimated model parameters and  $\widetilde{\mathbf{C}}_m$  the covariance matrix representing the uncertainties of the estimated model parameters. As a typical choice (e.g., [Lohman, 2004](#); [Delouis et al., 2010](#); [Awaluddin et al., 2012](#); [Tung and Masterlark, 2016](#); [Yáñez-Cuadra et al., 2023](#)), we use  $\mathbf{H} = \nabla^2$ , a Laplacian operator, to define a slip smoothing constraint, aimed to deal with the inherent instability of the slip inversion. We refer the reader to [Ortega-Culaciati et al. \(2021\)](#) and references therein, for further details on the Linear Least Squares method

and on the effectiveness of the variety of regularization types that can be defined to deal with the inherent instabilities of the quasi-static slip estimation problem.

When estimating the coseismic slip distribution of a megathrust earthquake, it is generally expected that slip on each subfault will exhibit a reverse (updip) direction. As a result, imposing a positivity constraint on the dip-slip component becomes a natural requirement, leading to the following inverse problem:

$$\begin{aligned} \min_{\mathbf{m}} \quad & \|\mathbf{W}_d(\mathbf{G}\mathbf{m} - \mathbf{d})\|_2^2 + \varepsilon^2 \|\mathbf{H}\mathbf{m}\|_2^2 \\ \text{subject to} \quad & \mathbf{m}_\delta \geq 0. \end{aligned} \quad (5)$$

where  $\mathbf{m}_\delta$  refers to the subset of  $\mathbf{m}$  representing the dip component of slip at each subfault. To solve this problem 5, we apply a trust-region reflective method ([Coleman and Li, 1996](#)), which allows for the definition of bounds constraints on a specific subset of model parameters,  $\mathbf{m}$ . In the Discussion section, we will compare this method with the proposed neural network model.

## 2.3 Artificial Neural Networks

Artificial Neural Networks (ANNs) are a type of Machine Learning method inspired by the structure and function of the human brain, capable of solving complex problems through interconnected layers of neurons. In general, a neural network comprises an input layer, one or more hidden layers, and an output layer. The input layer receives the data, the hidden layers process it by extracting patterns and features through a series of computations, and the output layer delivers the final result—mimicking the flow of information in neural pathways (e.g., [Wang, 2003](#); [Goodfellow et al., 2016](#)).

In our study, we use a neural network as the predictive model to estimate earthquake slip distributions. Specifically, the network is trained to learn the relationship between surface crustal displacements (recorded at GNSS sites) and their causative fault slip distributions, using a large synthetic dataset of earthquake scenarios. During training, an optimization algorithm iteratively adjusts the internal parameters (weights and biases) via backpropagation ([Yegnanarayana, 2009](#)) to minimize a loss function. The training data are split into batches and processed over several epochs, allowing the network to gradually refine its predictions. Once trained, the network can predict fault slip distributions from new displacement data it has not previously seen.

The architecture of our preferred model is straightforward, consisting of just one hidden layer with 100 neurons, alongside the input and output layers. The input layer receives surface crustal displacements at the location of GNSS sites, and the output layer predicts quantities that will be later translated into a fault slip distribution. To prevent overfitting, we incorporate a dropout layer with a 35% rate between the hidden and output layers. In our dense layers, each neuron is connected to every neuron in both the preceding and subsequent layers.

For the activation function in the hidden layer, we employ the Gaussian Error Linear Unit (GELU) ([Hendrycks D., 2016](#)), which serves as a smoother alternative to the traditional ReLU ([Krizhevsky et al., 2017](#)).

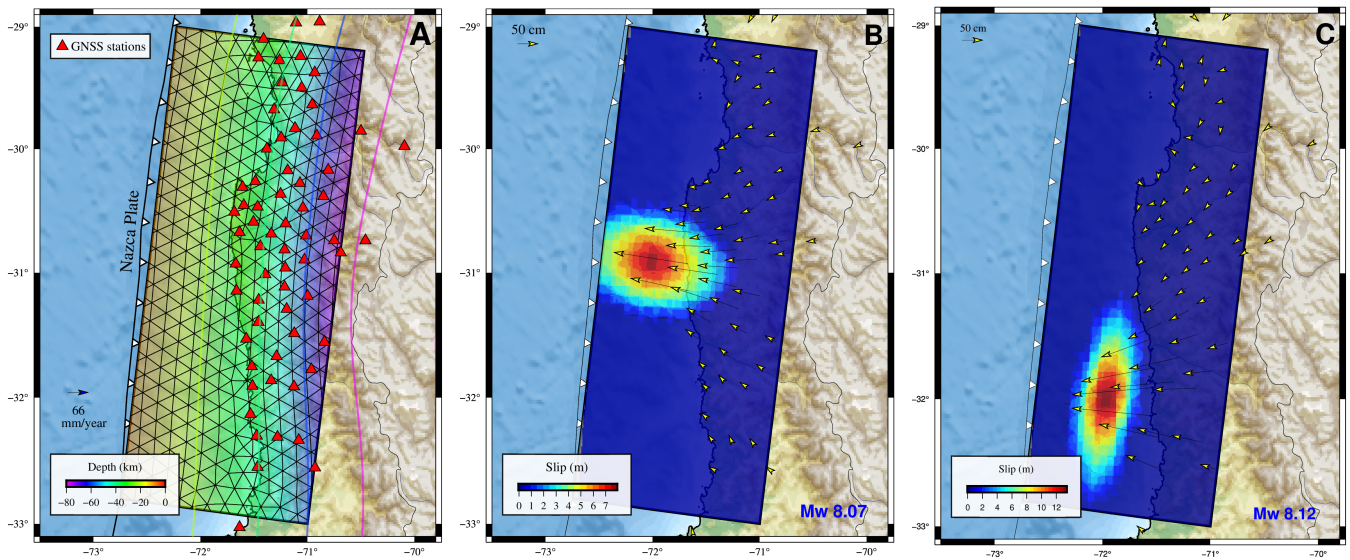


**Figure 1** (a) Representation of the configuration used, including the SLAB 2.0 model for the subduction megathrust geometry and the triangular mesh discretization. The red triangles indicate the distribution of GNSS stations. (b) Example of a synthetic earthquake scenario showing the corresponding slip distribution. (c) A second synthetic scenario with a different slip distribution.

GELU is mathematically defined as:

$$\text{GELU}(x) = x \Phi(x), \quad (6)$$

where  $\Phi(x)$  represents the cumulative distribution function of the standard Gaussian. This non-linear function weights the input  $x$  by the probability that  $x$  is less than or equal to itself, thus enabling gradual adjustment of the outputs. In the output layer, we use the sigmoid function to transform the outputs into the range  $[0, 1]$ :

$$\text{Sigmoid}(x) = \frac{1}{1 + e^{-x}}. \quad (7)$$

Additionally, we tested different activation functions, including ReLU (Krizhevsky et al., 2017), SELU (Klambauer et al., 2017), Mish (Misra, 2019), ELU (Clevert et al., 2015), and Swish (Ramachandran et al., 2017). For further details on these experiments, the reader is referred to the supplementary material.

The network was implemented and trained using the *TensorFlow* library (Abadi et al., 2015). Prior to training, the data were normalized using min-max scaling to ensure that all values fell within the 0 to 1 range, thereby optimizing the efficiency of the learning process. Our training dataset comprises 300,000 synthetic cases (as detailed in Section 2.1), partitioned into 80% for training and 20% for testing, with 10% of the training set further allocated for validation. The network was trained over 10 epochs using the Adam optimizer (Kingma and Ba, 2014) to minimize the Mean Squared Error (MSE):

$$\text{MSE} = \frac{1}{n} \sum_{i=1}^n (y_i - \hat{y}_i)^2, \quad (8)$$

where  $y_i$  and  $\hat{y}_i$  denote the actual and predicted slip values, respectively, and  $n$  is the total number of samples. Performance was further evaluated using the Root

Mean Squared Error (RMSE) and the Mean Absolute Error (MAE):

$$\text{RMSE} = \sqrt{\frac{1}{n} \sum_{i=1}^n (y_i - \hat{y}_i)^2}, \quad \text{MAE} = \frac{1}{n} \sum_{i=1}^n |y_i - \hat{y}_i|. \quad (9)$$

After training, the network's outputs were rescaled to their original range using the same normalization parameters.

## 3 Results

### 3.1 Synthetic case

Initially, we tested our model on the synthetic cases we developed. The model demonstrates the capability to capture the coseismic slip, aligning closely with the anticipated magnitudes, with minor discrepancies in the slip distribution (as shown in Fig. 2). The predicted slip tends to be smaller and more concentrated in the center. This pattern, which appears consistently across all synthetic cases, indicates a slight underestimation in the slip distribution. The mean RMSE for the GNSS displacements of the synthetic cases is 0.13 m, while the mean MAE is 0.06 m.

### 3.2 Illapel case

Using our preferred model to estimate the coseismic slip of the Illapel earthquake (Figure 2), we found that the mainshock slip distribution spans from 30.3°S to 31.9°S in latitude and from 72.6°W to 71.1°W in longitude. The peak coseismic slip reached 9 meters, with an along-strike rupture length of approximately 177 km (Figure 3). The slip distribution yields a geodetic seismic moment of  $M_o = 3.35 \times 10^{21}$  Nm, equivalent to an  $M_w = 8.32$  earthquake.

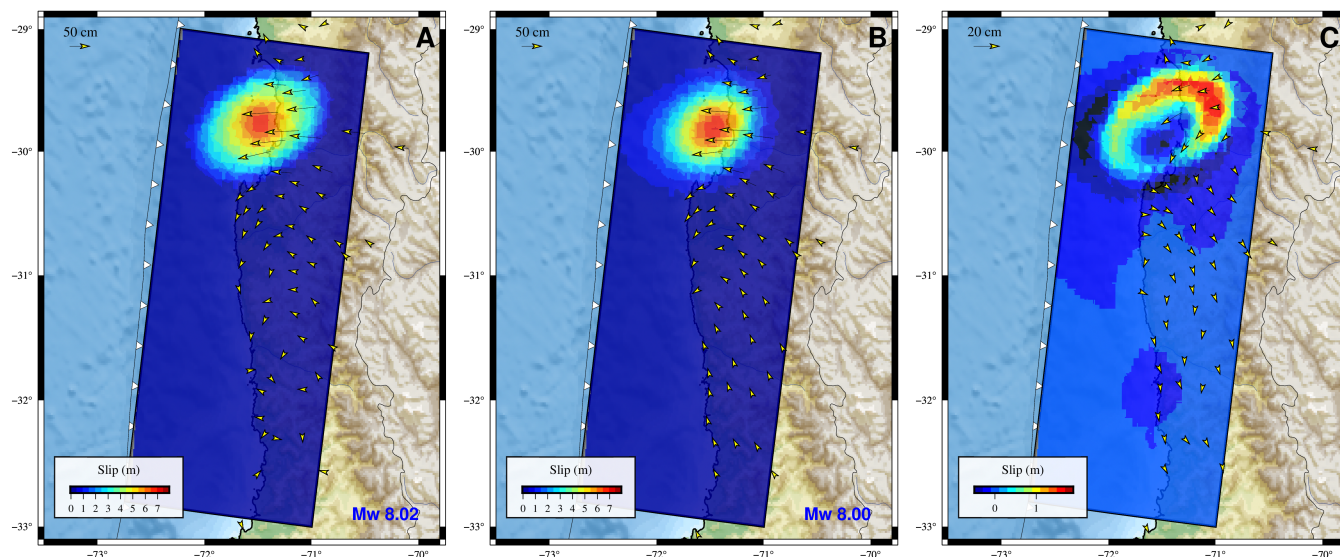


**Figure 2** Example of a synthetic case: (a) Slip distribution with displacement vectors shown in yellow for a synthetic scenario; magnitude and RMSE details displayed in the bottom right. (b) Model prediction for the synthetic case. (c) Residuals and slip differences for the presented synthetic case.

Regarding the GNSS displacement vectors in the horizontal components, they are generally well-recovered from the original data but are slightly more oriented towards the south and larger than expected (i.e., measured) values. Similarly, the vertical components are accurately captured but also appear slightly larger than anticipated, as shown in Figure S1. Despite these discrepancies, the overall recovery of the displacement vectors is notably accurate in both components. For the horizontal components, the average residual is 3.5 cm, while for the vertical components, it is 1.6 cm, which we consider acceptable given the maximum displacement values of approximately 2 meters.

### 3.3 Analysis of impact of hyperparameters and data conditions

In this section, we demonstrate the impact of both model hyperparameters and experimental conditions on the estimation of coseismic slip for the Illapel case. To ensure a consistent comparison, we maintained the same data volume and architecture across all models, modifying only the necessary parameters or conditions. Specifically, we explored the influence of the choice of activation function for the hidden layer, the dropout rate, and the number of training epochs. Concurrently, we examined various experimental conditions critical to our study. We utilized a subset of only 13 GNSS stations, as described by Shrivastava et al. (2016), to understand the impact of the number of GNSS stations on the model performance. We also varied the volume of synthetic cases used for training. Additionally, to assess the model's robustness, we introduced noise to the GNSS training data. Although such noise is not considered as a hyperparameter, its incorporation is crucial in defining the training environment and data characteristics that influence model training and performance. The results of this analysis are presented in Fig. 4 and additionally in Figures S2 to S9.

With respect to activation functions, Mish demonstrated the second-best performance after GELU (Figure 4a), followed by SELU, while ReLU and Swish exhibited the poorest performance. This trend is reflected in both the metric values and residual analysis as shown in Figures S2 and S3. Although most activation functions tend to overestimate slip, the GELU function used in the preferred model is capable of accurately recovering it. This can be attributed to GELU's smooth probabilistic curve, which preserves gradient information better than other activation functions. Further details on the performance of other activation functions can be found in the supplementary material.

The dropout rate plays a crucial role in enhancing the model ability to generalize by mitigating overfitting. Intermediate dropout rates between 30 and 50% perform better, as evidenced in Figures S4 and S5. In contrast, lower dropout rates, such as 10 to 20%, lead to higher RMSE and MAE values, and higher residuals (Figure 4b). Conversely, higher dropout rates help to smooth the results but can mask finer details in the data. A dropout rate of 35% is considered to be the most effective in this case, achieving the best balance.

Changing the number of training epochs did not result in significant changes in RMSE, MAE, or residuals (Figures 4c, S6, and S7). The lack of a clear pattern suggests that increasing the number of epochs does not lead to better model performance. This analysis identifies the activation function as the most critical hyperparameter for our model, followed by the dropout rate and the number of training epochs.

In terms of data conditions, the reduction in the number of GNSS stations negatively impacted the model performance, leading to higher RMSE and MAE values. Despite this, the model was still able to reasonably estimate the slip magnitude and distribution, although with larger uncertainties due to the sparsely-distributed stations (Figure 4d). As expected, the use of more syn-

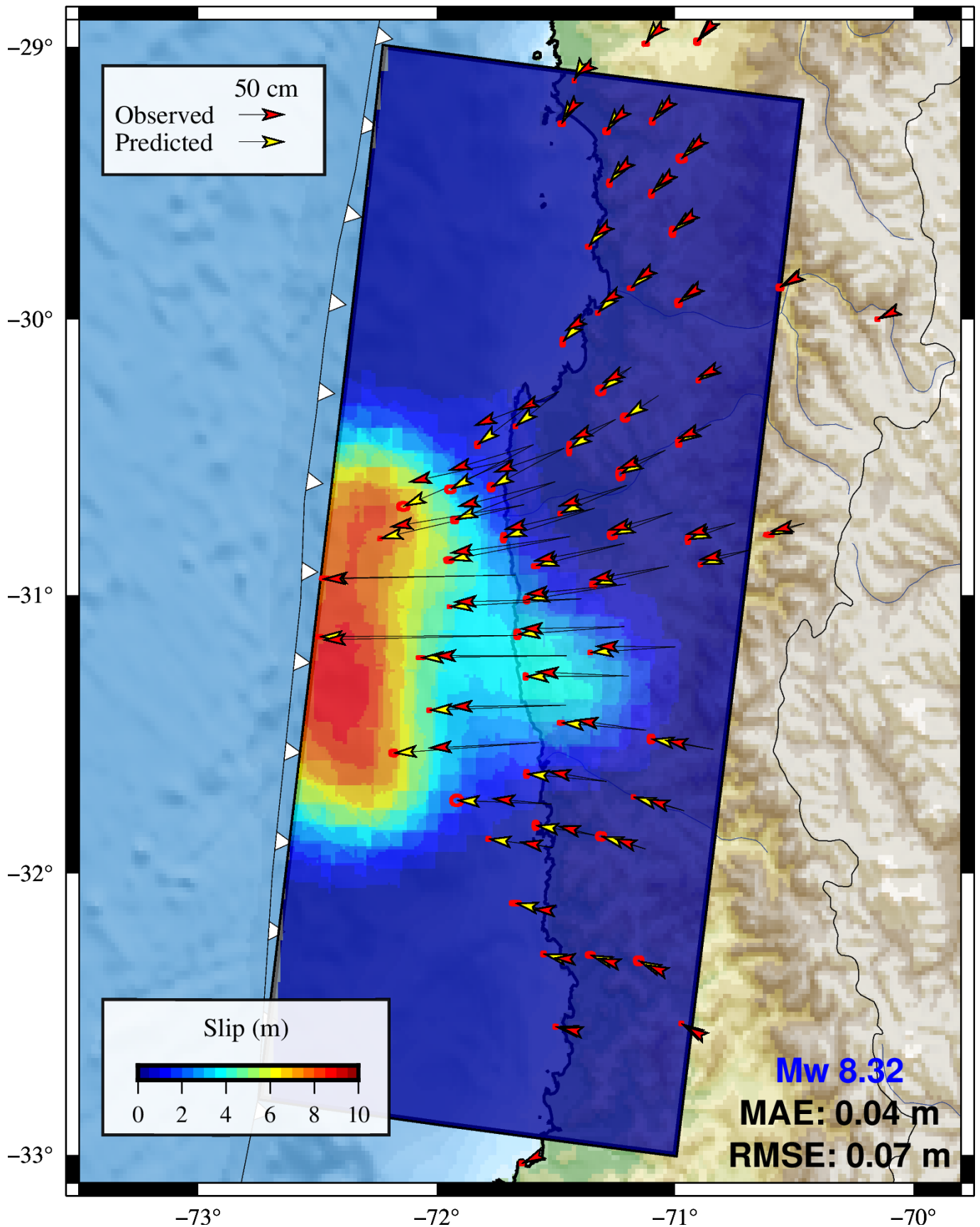


**Figure 3** Estimated coseismic slip distribution for the Illapel earthquake using our preferred model, showing displacement vectors. Predicted vectors are in yellow, observed vectors are in red, and 95% confidence intervals are included as red ellipses to illustrate the uncertainties in the model predictions.

thetic cases resulted in better performance (Figures S8 and S9), indicating that at least 200,000 synthetic cases for training are needed for robust results (Figure 4e).

Introducing noise confirmed the model robustness, as it still accurately estimated coseismic slip and magnitude as shown in Figure 4f.

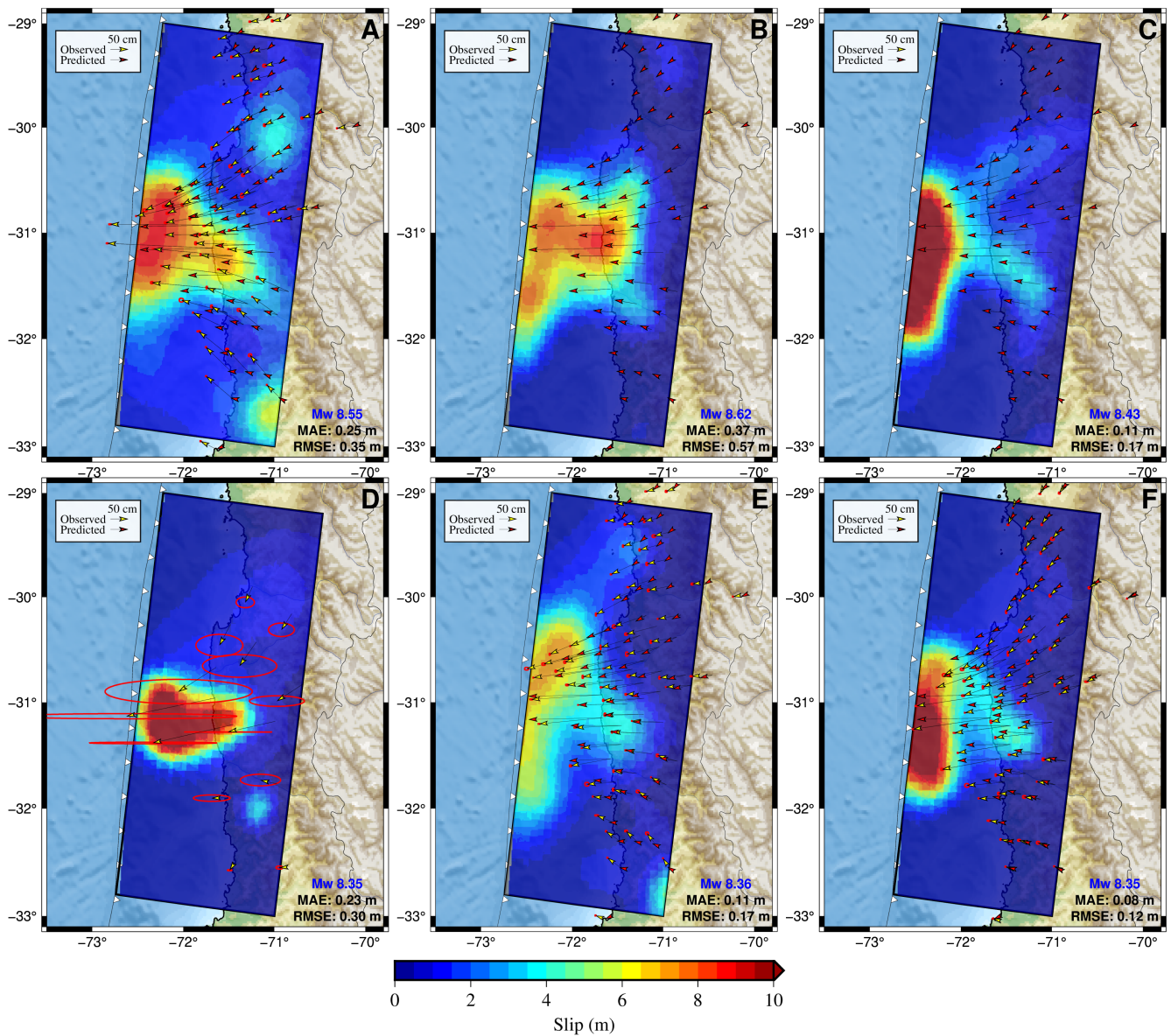


**Figure 4** Impact of different hyperparameters and experimental conditions on coseismic slip estimation for the Illapel case. Each panel displays the predicted and observed displacement vectors, with predictions in yellow and observations in red. The panels also include 95% confidence ellipses illustrating the uncertainty in the predictions. Subfigures show the effects of: (a) Mish activation function in the hidden layer, (b) 20% dropout rate, (c) 50 training epochs, (d) using 13 only GNSS stations, (e) training with 200,000 synthetic cases, (f) introducing noise into the training data.

## 4 Discussion

The preferred neural network model, tested on the Illapel earthquake, is consistent with the slip distribution estimated in other studies. Our model maximum slip (9 m) is consistent with the estimates from Melgar et al. (2016), Klein et al. (2017), and Zhang et al. (2017) (10 m); Shrivastava et al. (2016) (8 m); Williamson et al. (2017) (11 m); and Carrasco et al. (2019) (9 m). The along-strike length of the slip (177 km) is similar to other studies: Zhang et al. (2017) (170km); Klein et al. (2017), Melgar et al. (2016), and Shrivastava et al. (2016) (200 km); Williamson et al. (2017) (125 km); and Carrasco et al. (2019) (180 km). Furthermore, the seismic moment in our model ( $3.66 \times 10^{21}$  Nm, i.e.  $M_w$  8.32) is consistent with the USGS W-phase model of  $3.19 \times 10^{21}$  Nm, i.e.

$M_w$  8.27.

Comparing our preferred model with an inversion using the Regularized Least Squares (RLS) method, we observed that our model exhibits higher residuals. Specifically, the root mean square (RMS) of the GNSS data residuals for our model is 6 cm, compared to 2.2 cm for the RLS inversion model. As illustrated in Fig. 5, the RLS inversion model consistently shows lower residuals across the study area. This discrepancy is particularly noticeable in the southern zone, where our model residuals are significantly higher, as seen in Figure 5a and Figure 5b. This may be attributed to the distribution of GNSS stations, as the higher station density in the northern region provides better constraints for the model, resulting in lower residuals. The GNSS data residual graph (Figures 5c and 5d) indicates that residuals from our

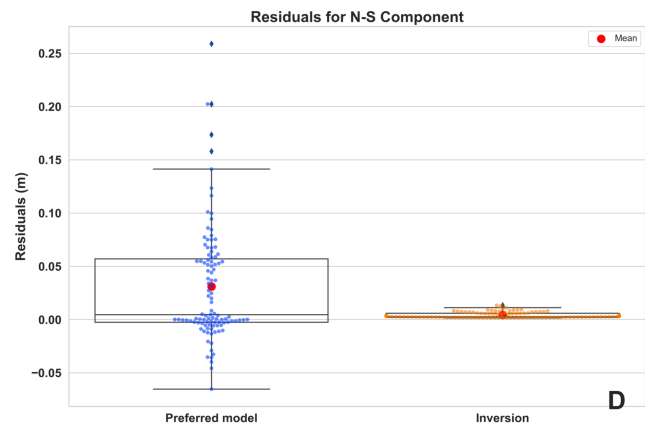
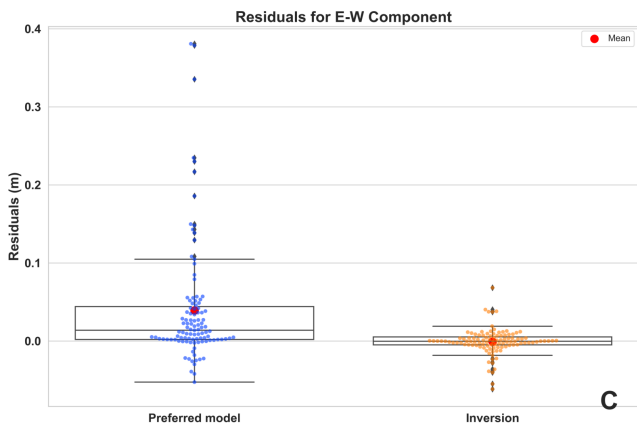
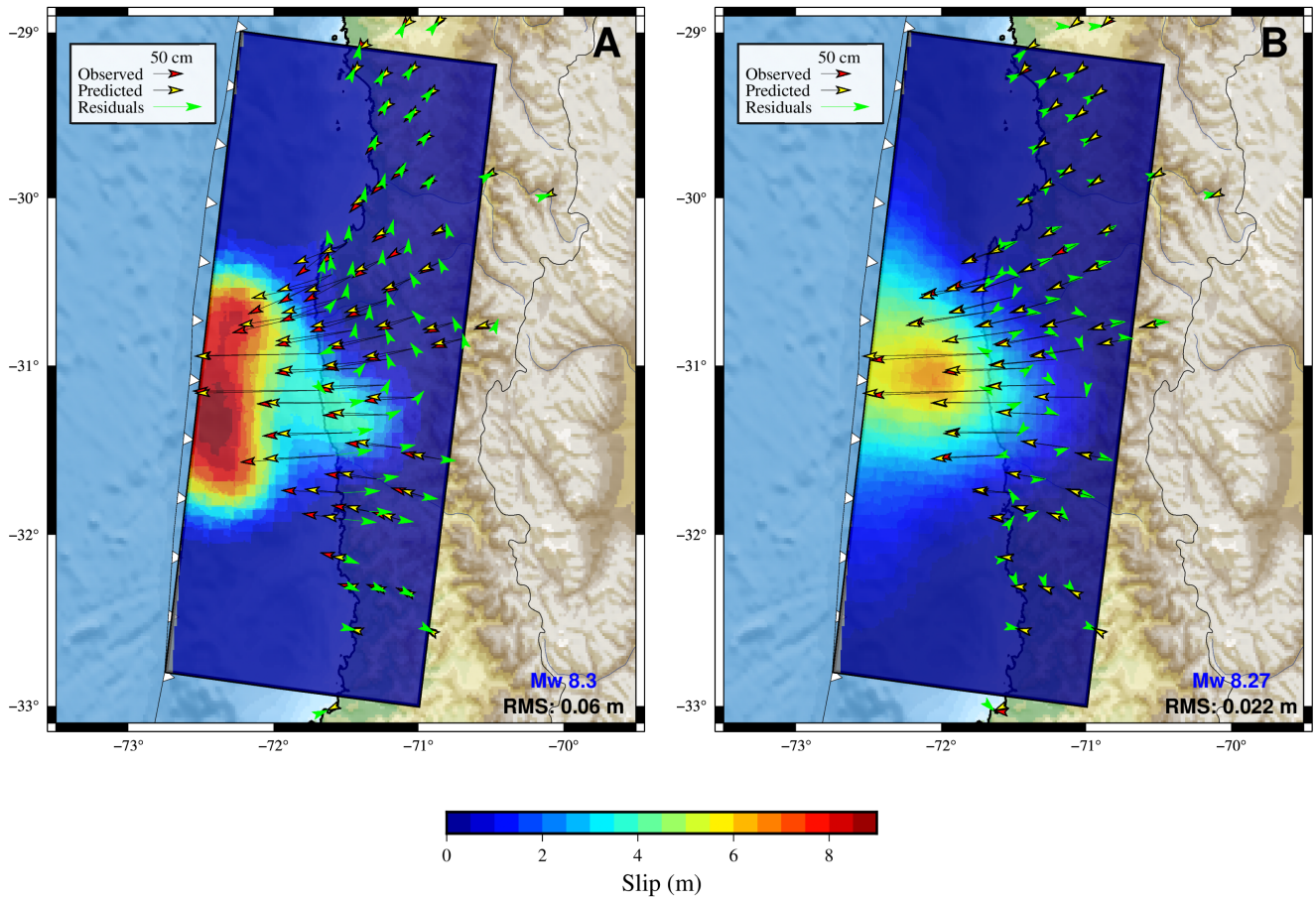


**Figure 5** (a) Preferred model slip distribution with residuals highlighted in green. (b) Slip distribution from Regularized Least Squares inversion. (c) Comparison of East-West (E-W) component residuals for the preferred model (in blue) and classic inversion (in orange). (d) Comparison of North-South (N-S) component residuals across both models.

model are more dispersed and include more extreme values, although their values are generally distributed around 0 cm. The vertical components exhibit lower residuals compared to the horizontal components, as detailed in Figure S10.

Furthermore, a significant observation from our model is the estimation of substantial slip close to the

trench, contrasting with the inversion model slip, which is positioned further away from the trench. This finding aligns with the slip patterns noted by Carrasco et al. (2019) and Caballero et al. (2023), where the slip is also estimated near the trench and is consistent with the tsunami observations of Lay et al. (2016), underscoring a possible area-specific frictional behavior at the sub-

duction megathrust that our model captures more effectively, even though is constrained only by on-land GNSS observations.

## 5 Conclusions

In this study, we developed a novel neural network model that rapidly and accurately estimates coseismic slip. The model demonstrated high accuracy in predicting both the magnitude and spatial distribution of slip for synthetic cases, and was subsequently validated with the Mw 8.3 Illapel earthquake, achieving a GNSS displacement RMSE of 0.07 m and showing consistency with previously published solutions. This capability is essential for improving early warning systems and advancing real-time seismic hazard assessments.

A standout feature of our approach is its computational efficiency: once trained, the model generates slip estimations in just 0.07 seconds on a conventional computer without requiring iterative model tuning, significantly simplifying the estimation process. These computations were performed on a standard personal computer equipped with an AMD Ryzen 5 5600G processor and 16 GB of RAM, without the use of a dedicated GPU. This speed, combined with minimal hardware requirements, highlights the potential of neural networks to help with quick earthquake response and risk mitigation.

The impact of hyperparameters and data conditions on model performance was evident. Among the activation functions tested, GELU produced the most accurate slip magnitudes, while others tended to overestimate. Dropout rates between 30% and 50% improved generalization, and varying the number of training epochs had little effect. Reducing the number of GNSS stations and synthetic cases increased errors, reinforcing their importance for model accuracy. Despite the added noise, the model remained robust, consistently delivering reliable slip estimates.

Performance analysis showed that the East-West component of slip had the highest residuals and variability, indicating more potential errors in this direction. The North-South component followed, while the vertical component showed the lowest variability, likely due to its smaller magnitude, making it easier for the neural network to learn. Although the horizontal components generally have higher accuracy in GNSS measurements, their larger magnitudes seem to pose a greater challenge for the model, leading to higher residuals compared to the vertical component. These patterns suggest specific areas where the model could be further improved.

However, the model applicability is inherently limited by the distribution of GNSS stations used for training, as station density directly affects its ability to resolve slip patterns. Furthermore, the model was trained exclusively on single-asperity earthquakes, making it well-suited for events with similar rupture characteristics. Expanding its applicability to more complex, multi-asperity earthquakes would require a broader and more diverse training dataset, as well as exploring more complex neural network architectures. To develop a

more generalizable model capable of predicting slip for various megathrust earthquakes in Chile, it would be necessary to incorporate data from all available GNSS stations in the region and a wider range of rupture scenarios.

Ultimately, while the model performs well for single-asperity events and offers significant computational advantages, enhancing its training dataset with more synthetic cases and realistic rupture patterns would strengthen its predictive accuracy. Incorporating more diverse scenarios, particularly ellipses that closely resemble real events, could further improve model reliability. These refinements would contribute to developing a more versatile tool for estimating coseismic slip across a broader spectrum of seismic events.

## Acknowledgements

This study was supported by the project FONDECYT 1221507. F.O.-C. acknowledges support from project FONDECYT 1231684. We also acknowledge the use of Generic Mapping Tools (GMT), developed by [Wessel and Smith \(1998\)](#), for the creation of the figures presented in this paper. We gratefully acknowledge the support of the Geophysics Master's program at the University of Concepción. We sincerely thank the anonymous reviewers for their constructive comments and suggestions, which have greatly improved the quality of this study.

## Data and code availability

The GNSS data used in this paper are available from [Klein et al. \(2017\)](#). The codes used for this study are available on Zenodo ([Inzunza, 2025](#)).

## Competing interests

The authors declare that there are no known financial or personal conflicts of interest that could have influenced the work reported in this paper.

## References

- Abadi, M., Agarwal, A., Barham, P., Brevdo, E., Chen, Z., Citro, C., Corrado, G. S., Davis, A., Dean, J., Devin, M., Ghemawat, S., Goodfellow, I., Harp, A., Irving, G., Isard, M., Jia, Y., Jozefowicz, R., Kaiser, L., Kudlur, M., Levenberg, J., Mané, D., Monga, R., Moore, S., Murray, D., Olah, C., Schuster, M., Shlens, J., Steiner, B., Sutskever, I., Talwar, K., Tucker, P., Vanhoucke, V., Vasudevan, V., Viégas, F., Vinyals, O., Warden, P., Wattenberg, M., Wicke, M., Yu, Y., and Zheng, X. TensorFlow: Large-Scale Machine Learning on Heterogeneous Systems [software], 2015. <https://www.tensorflow.org/>.
- Altamimi, Z., Reischung, P., Métivier, L., and Collilieux, X. ITRF2014: A new release of the International Terrestrial Reference Frame modeling nonlinear station motions. *Journal of Geophysical Research: Solid Earth*, 121(8):6109–6131, Aug. 2016. doi: 10.1002/2016jb013098.
- Aster, R. C., Borchers, B., and Thurber, C. H. *Parameter estimation and inverse problems*. Elsevier, 2013. doi: 10.1016/c2009-0-61134-x.

- Awaluddin, M., Meilano, I., and Widiyantoro, S. Estimation of Slip Distribution of the 2007 Bengkulu Earthquake from GPS Observations Using the Least-Squares Inversion Method. *ITB Journal of Engineering Science*, 44(2):187–206, 2012. doi: 10.5614/itbj.eng.sci.2012.44.2.6.
- Barra, S., Moreno, M., Ortega-Culaciati, F., Benavente, R., Araya, R., Bedford, J., and Calisto, I. A supervised machine learning approach for estimating plate interface locking: Application to Central Chile. *Physics of the Earth and Planetary Interiors*, 352: 107207, July 2024. doi: 10.1016/j.pepi.2024.107207.
- Barrientos, S. E. and Ward, S. N. The 1960 Chile earthquake: inversion for slip distribution from surface deformation. *Geophysical Journal International*, 103(3):589–598, Dec. 1990. doi: 10.1111/j.1365-246x.1990.tb05673.x.
- Bedford, J., Moreno, M., Baez, J. C., Lange, D., Tilmann, F., Rose- nau, M., Heibach, O., Oncken, O., Bartsch, M., Rietbrock, A., Tassara, A., Bevis, M., and Vigny, C. A high-resolution, time-variable afterslip model for the 2010 Maule Mw = 8.8, Chile megathrust earthquake. *Earth and Planetary Science Letters*, 383:26–36, Dec. 2013. doi: 10.1016/j.epsl.2013.09.020.
- Caballero, E., Duputel, Z., Twardzik, C., Rivera, L., Klein, E., Jiang, J., Liang, C., Zhu, L., Jolivet, R., Fielding, E., and Simons, M. Revisiting the 2015 Mw = 8.3 Illapel earthquake: unveiling complex fault slip properties using Bayesian inversion. *Geophysical Journal International*, 235(3):2828–2845, Sept. 2023. doi: 10.1093/gji/ggad380.
- Carr Agnew, D. Realistic Simulations of Geodetic Network Data: The Fakenet Package. *Seismological Research Letters*, 84(3): 426–432, May 2013. doi: 10.1785/0220120185.
- Carrasco, S., Ruiz, J. A., Contreras-Reyes, E., and Ortega-Culaciati, F. Shallow intraplate seismicity related to the Illapel 2015 Mw 8.4 earthquake: Implications from the seismic source. *Tectonophysics*, 766:205–218, Sept. 2019. doi: 10.1016/j.tecto.2019.06.011.
- Chen, K., Ge, M., Li, X., Babeyko, A., Ramatschi, M., and Bradke, M. Retrieving real-time precise co-seismic displacements with a standalone single-frequency GPS receiver. *Advances in Space Research*, 56(4):634–647, Aug. 2015. doi: 10.1016/j.asr.2015.04.029.
- Chlieh, M., Avouac, J.-P., Hjorleifsdottir, V., Song, T.-R. A., Ji, C., Sieh, K., Sladen, A., Hebert, H., Prawirodirdjo, L., Bock, Y., and Galetzka, J. Coseismic Slip and Afterslip of the Great  $M_w$  9.15 Sumatra–Andaman Earthquake of 2004. *Bulletin of the Seismological Society of America*, 97(1A):S152–S173, Jan. 2007. doi: 10.1785/0120050631.
- Cisternas, M., Carvajal, M., Wesson, R., Ely, L. L., and Gorigoitia, N. Exploring the Historical Earthquakes Preceding the Giant 1960 Chile Earthquake in a Time-Dependent Seismogenic Zone. *Bulletin of the Seismological Society of America*, 107(6):2664–2675, Nov. 2017. doi: 10.1785/0120170103.
- Clevert, D.-A., Unterthiner, T., and Hochreiter, S. Fast and Accurate Deep Network Learning by Exponential Linear Units (ELUs), 2015. doi: 10.48550/ARXIV.1511.07289.
- Coleman, T. F. and Li, Y. An Interior Trust Region Approach for Non-linear Minimization Subject to Bounds. *SIAM Journal on Optimization*, 6(2):418–445, May 1996. doi: 10.1137/0806023.
- Craven, P. and Wahba, G. Smoothing noisy data with spline functions: Estimating the correct degree of smoothing by the method of generalized cross-validation. *Numerische Mathematik*, 31(4):377–403, Dec. 1978. doi: 10.1007/bf01404567.
- Cui, W., Chen, K., Wei, G., Lyu, M., and Zhu, F. Simultaneous magnitude and slip distribution characterization from high-rate GNSS using deep learning: case studies of the 2021 Mw 7.4 Maduo and 2023 Turkey doublet events. *Geophysical Journal International*, 238(1):91–108, Apr. 2024. doi: 10.1093/gji/ggae140.
- Delouis, B., Nocquet, J., and Vallée, M. Slip distribution of the February 27, 2010 Mw = 8.8 Maule Earthquake, central Chile, from static and high-rate GPS, InSAR, and broadband teleseismic data. *Geophysical Research Letters*, 37(17), Sept. 2010. doi: 10.1029/2010gl043899.
- Donoso, F., Moreno, M., Ortega-Culaciati, F., Bedford, J. R., and Benavente, R. Automatic Detection of Slow Slip Events Using the PICCA: Application to Chilean GNSS Data. *Frontiers in Earth Science*, 9, Dec. 2021. doi: 10.3389/feart.2021.788054.
- Duputel, Z., Agram, P. S., Simons, M., Minson, S. E., and Beck, J. L. Accounting for prediction uncertainty when inferring subsurface fault slip. *Geophysical Journal International*, 197(1): 464–482, Jan. 2014. doi: 10.1093/gji/ggt517.
- Duputel, Z., Jiang, J., Jolivet, R., Simons, M., Rivera, L., Ampuero, J., Riel, B., Owen, S. E., Moore, A. W., Samsonov, S. V., Ortega Culaciati, F., and Minson, S. E. The Iquique earthquake sequence of April 2014: Bayesian modeling accounting for prediction uncertainty. *Geophysical Research Letters*, 42(19):7949–7957, Oct. 2015. doi: 10.1002/2015gl065402.
- Fujii, Y. and Satake, K. Slip Distribution and Seismic Moment of the 2010 and 1960 Chilean Earthquakes Inferred from Tsunami Waveforms and Coastal Geodetic Data. *Pure and Applied Geophysics*, 170(9–10):1493–1509, Aug. 2012. doi: 10.1007/s00024-012-0524-2.
- Fujii, Y., Satake, K., Sakai, S., Shinohara, M., and Kanazawa, T. Tsunami source of the 2011 off the Pacific coast of Tohoku Earthquake. *Earth, Planets and Space*, 63(7):815–820, July 2011. doi: 10.5047/eps.2011.06.010.
- Goodfellow, I., Bengio, Y., and Courville, A. *Deep Learning*. MIT Press, 2016. <http://www.deeplearningbook.org>.
- Hansen, P. C. and O’Leary, D. P. The Use of the L-Curve in the Regularization of Discrete Ill-Posed Problems. *SIAM Journal on Scientific Computing*, 14(6):1487–1503, Nov. 1993. doi: 10.1137/0914086.
- Harris, R. A. and Segall, P. Detection of a locked zone at depth on the Parkfield, California, segment of the San Andreas Fault. *Journal of Geophysical Research: Solid Earth*, 92(B8):7945–7962, July 1987. doi: 10.1029/jb092ib08p07945.
- Hayes, G. P., Moore, G. L., Portner, D. E., Hearne, M., Flamme, H., Furtney, M., and Smoczyk, G. M. Slab2, a comprehensive subduction zone geometry model. *Science*, 362(6410):58–61, Oct. 2018. doi: 10.1126/science.aat4723.
- Heidarzadeh, M., Murotani, S., Satake, K., Ishibe, T., and Gusman, A. R. Source model of the 16 September 2015 Illapel, Chile, Mw 8.4 earthquake based on teleseismic and tsunami data. *Geophysical Research Letters*, 43(2):643–650, Jan. 2016. doi: 10.1002/2015gl067297.
- Hendrycks D., Gimpel, K. Gaussian error linear units (GELUs). *arXiv Preprint, arXiv:1606.08415*, 2016.
- Iinuma, T., Hino, R., Kido, M., Inazu, D., Osada, Y., Ito, Y., Ohzono, M., Tsushima, H., Suzuki, S., Fujimoto, H., and Miura, S. Coseismic slip distribution of the 2011 off the Pacific Coast of Tohoku Earthquake (M9.0) refined by means of seafloor geodetic data. *Journal of Geophysical Research: Solid Earth*, 117(B7), July 2012. doi: 10.1029/2012jb009186.
- Inzunza, V. Supplementary Materials for “Application of Neural Networks for Estimating Coseismic Slip Distribution Using Synthetic GNSS Data”, 2025. doi: 10.5281/zenodo.14051275.
- Jara, J., Sánchez-Reyes, H., Socquet, A., Cotton, F., Virieux, J., Maksymowicz, A., Díaz-Mojica, J., Walpersdorf, A., Ruiz, J., Cotte, N., and Norabuena, E. Kinematic study of Iquique 2014 M 8.1 earthquake: Understanding the segmentation of the

- seismogenic zone. *Earth and Planetary Science Letters*, 503: 131–143, Dec. 2018. doi: 10.1016/j.epsl.2018.09.025.
- Kingma, D. and Ba, J. Adam: A Method for Stochastic Optimization. *International Conference on Learning Representations*, 12 2014.
- Klambauer, G., Unterthiner, T., Mayr, A., and Hochreiter, S. Self-Normalizing Neural Networks. 2017. doi: 10.48550/ARXIV.1706.02515.
- Klein, E., Vigny, C., Fleitout, L., Grandin, R., Jolivet, R., Rivera, E., and Métois, M. A comprehensive analysis of the Illapel 2015 Mw8.3 earthquake from GPS and InSAR data. *Earth and Planetary Science Letters*, 469:123–134, July 2017. doi: 10.1016/j.epsl.2017.04.010.
- Krizhevsky, A., Sutskever, I., and Hinton, G. E. ImageNet classification with deep convolutional neural networks. *Communications of the ACM*, 60(6):84–90, May 2017. doi: 10.1145/3065386.
- Lawson, C. L. and Hanson, R. J. *Solving Least Squares Problems*. Society for Industrial and Applied Mathematics, Jan. 1995. doi: 10.1137/1.9781611971217.
- Lay, T., Kanamori, H., Ammon, C. J., Nettles, M., Ward, S. N., Aster, R. C., Beck, S. L., Bilek, S. L., Brudzinski, M. R., Butler, R., DeShon, H. R., Ekström, G., Satake, K., and Sipkin, S. The Great Sumatra-Andaman Earthquake of 26 December 2004. *Science*, 308(5725): 1127–1133, May 2005. doi: 10.1126/science.1112250.
- Lay, T., Li, L., and Cheung, K. F. Modeling tsunami observations to evaluate a proposed late tsunami earthquake stage for the 16 September 2015 Illapel, Chile, Mw 8.3 earthquake. *Geophysical Research Letters*, 43(15):7902–7912, Aug. 2016. doi: 10.1002/2016gl070002.
- Lin, J., Melgar, D., Thomas, A. M., and Searcy, J. Early Warning for Great Earthquakes From Characterization of Crustal Deformation Patterns With Deep Learning. *Journal of Geophysical Research: Solid Earth*, 126(10), Oct. 2021. doi: 10.1029/2021jb022703.
- Lohman, R. B. *The Inversion of Geodetic Data for Earthquake Parameters*. PhD thesis, California Institute of Technology, 2004. doi: 10.7907/9FYH-HD84.
- Lorenzo-Martín, F., Roth, F., and Wang, R. Inversion for rheological parameters from post-seismic surface deformation associated with the 1960 Valdivia earthquake, Chile. *Geophysical Journal International*, 164(1):75–87, Jan. 2006. doi: 10.1111/j.1365-246x.2005.02803.x.
- Luo, H., Ambrosius, B., Russo, R. M., Mocanu, V., Wang, K., Bevis, M., and Fernandes, R. A recent increase in megathrust locking in the southernmost rupture area of the giant 1960 Chile earthquake. *Earth and Planetary Science Letters*, 537:116200, May 2020. doi: 10.1016/j.epsl.2020.116200.
- Melgar, D., Fan, W., Riquelme, S., Geng, J., Liang, C., Fuentes, M., Vargas, G., Allen, R. M., Shearer, P. M., and Fielding, E. J. Slip segmentation and slow rupture of the trench during the 2015, Mw8.3 Illapel, Chile earthquake. *Geophysical Research Letters*, 43(3):961–966, Feb. 2016. doi: 10.1002/2015gl067369.
- Meng, L., Huang, H., Bürgmann, R., Ampuero, J. P., and Strader, A. Dual megathrust slip behaviors of the 2014 Iquique earthquake sequence. *Earth and Planetary Science Letters*, 411:177–187, Feb. 2015. doi: 10.1016/j.epsl.2014.11.041.
- Menke, W. *Geophysical Data Analysis: Discrete Inverse Theory*. Academic Press, San Diego, California, 1989.
- Minson, S. E., Simons, M., and Beck, J. L. Bayesian inversion for finite fault earthquake source models I—theory and algorithm. *Geophysical Journal International*, 194(3):1701–1726, June 2013. doi: 10.1093/gji/ggt180.
- Misra, D. Mish: A Self Regularized Non-Monotonic Activation Function, 2019. doi: 10.48550/ARXIV.1908.08681.
- Moreno, M., Rosenau, M., and Oncken, O. 2010 Maule earthquake slip correlates with pre-seismic locking of Andean subduction zone. *Nature*, 467(7312):198–202, Sept. 2010. doi: 10.1038/nature09349.
- Moreno, M., Melnick, D., Rosenau, M., Baez, J., Klotz, J., Oncken, O., Tassara, A., Chen, J., Bataille, K., Bevis, M., Socquet, A., Bolte, J., Vigny, C., Brooks, B., Ryder, I., Grund, V., Smalley, B., Carrizo, D., Bartsch, M., and Hase, H. Toward understanding tectonic control on the Mw 8.8 2010 Maule Chile earthquake. *Earth and Planetary Science Letters*, 321–322:152–165, Mar. 2012. doi: 10.1016/j.epsl.2012.01.006.
- Münchmeyer, J., Giffard-Roisin, S., Malfante, M., Frank, W., Poli, P., Marsan, D., and Socquet, A. Deep learning detects uncataloged low-frequency earthquakes across regions. *Seismica*, 3(1), May 2024. doi: 10.26443/seismica.v3i1.1185.
- Nikkhoo, M. and Walter, T. R. Triangular dislocation: an analytical, artefact-free solution. *Geophysical Journal International*, 201(2):1119–1141, Mar. 2015. doi: 10.1093/gji/ggv035.
- Okada, Y. Surface deformation due to shear and tensile faults in a half-space. *Bulletin of the Seismological Society of America*, 75 (4):1135–1154, Aug. 1985. doi: 10.1785/bssa0750041135.
- Okal, E. A. and Stein, S. Observations of ultra-long period normal modes from the 2004 Sumatra–Andaman earthquake. *Physics of the Earth and Planetary Interiors*, 175(1–2):53–62, June 2009. doi: 10.1016/j.pepi.2009.03.002.
- Ortega-Culaciati, F., Simons, M., Ruiz, J., Rivera, L., and Díaz-Salazar, N. An EPIC Tikhonov Regularization: Application to Quasi-Static Fault Slip Inversion. *Journal of Geophysical Research: Solid Earth*, 126(7), June 2021. doi: 10.1029/2020jb021141.
- Ozawa, S., Nishimura, T., Munekane, H., Suito, H., Kobayashi, T., Tobita, M., and Imakiire, T. Preceding, coseismic, and post-seismic slips of the 2011 Tohoku earthquake, Japan. *Journal of Geophysical Research: Solid Earth*, 117(B7), July 2012. doi: 10.1029/2011jb009120.
- Ramachandran, P., Zoph, B., and Le, Q. V. Swish: a Self-Gated Activation Function, 2017. doi: 10.48550/ARXIV.1710.05941.
- Ruegg, J., Rudloff, A., Vigny, C., Madariaga, R., de Chabaliér, J., Campos, J., Kausel, E., Barrientos, S., and Dimitrov, D. Interseismic strain accumulation measured by GPS in the seismic gap between Constitución and Concepción in Chile. *Physics of the Earth and Planetary Interiors*, 175(1–2):78–85, June 2009. doi: 10.1016/j.pepi.2008.02.015.
- Shrivastava, M. N., González, G., Moreno, M., Chlieh, M., Salazar, P., Reddy, C. D., Báez, J. C., Yáñez, G., González, J., and de la Llera, J. C. Coseismic slip and afterslip of the 2015 Mw 8.3 Illapel (Chile) earthquake determined from continuous GPS data. *Geophysical Research Letters*, 43(20), Oct. 2016. doi: 10.1002/2016gl070684.
- Simons, M., Minson, S., Sladen, A., Ortega Culaciati, F., Jiang, J., Owen, S., Meng, L., Ampuero, J. P., Chu, R., Helmberger, D., Kanamori, H., Hetland, E., Moore, A., and Webb, F. The 2011 Magnitude 9.0 Tohoku-Oki Earthquake: Mosaicking the Megathrust from Seconds to Centuries. *Science*, 332, 2011. doi: 10.1126/science.1206731.
- Tajima, F., Mori, J., and Kennett, B. L. A review of the 2011 Tohoku-Oki earthquake (Mw 9.0): Large-scale rupture across heterogeneous plate coupling. *Tectonophysics*, 586:15–34, Feb. 2013. doi: 10.1016/j.tecto.2012.09.014.
- Tarantola, A. *Inverse Problem Theory and Methods for Model Parameter Estimation*. Society for Industrial and Applied Mathematics, Jan. 2005. doi: 10.1137/1.9780898717921.
- Thomas, A., Melgar, D., Dybing, S. N., and Searcy, J. R. Deep learning for denoising High-Rate Global Navigation Satellite System data. *Seismica*, 2(1), May 2023. doi: 10.26443/seismica.v2i1.240.

- Tilman, F., Zhang, Y., Moreno, M., Saul, J., Eckelmann, F., Palo, M., Deng, Z., Babeyko, A., Chen, K., Baez, J. C., Schurr, B., Wang, R., and Dahm, T. The 2015 Illapel earthquake, central Chile: A type case for a characteristic earthquake? *Geophysical Research Letters*, 43(2):574–583, Jan. 2016. doi: 10.1002/2015gl066963.
- Tung, S. and Masterlark, T. Coseismic slip distribution of the 2015 Mw7.8 Gorkha, Nepal, earthquake from joint inversion of GPS and InSAR data for slip within a 3-D heterogeneous Domain. *Journal of Geophysical Research: Solid Earth*, 121(5):3479–3503, May 2016. doi: 10.1002/2015jb012497.
- Wang, S.-C. *Interdisciplinary Computing in Java Programming*, chapter Artificial Neural Network. Springer US, 2003. doi: 10.1007/978-1-4615-0377-4.
- Wessel, P. and Smith, W. H. F. New, improved version of generic mapping tools released. *Eos, Transactions American Geophysical Union*, 79(47):579–579, Nov. 1998. doi: 10.1029/98eo00426.
- Williamson, A., Newman, A., and Cummins, P. Reconstruction of coseismic slip from the 2015 Illapel earthquake using combined geodetic and tsunami waveform data. *Journal of Geophysical Research: Solid Earth*, 122(3):2119–2130, Mar. 2017. doi: 10.1002/2016jb013883.
- Yegnanarayana, B. *Artificial Neural Networks*. PHI Learning Pvt. Ltd., New Delhi, 2009.
- Yáñez-Cuadra, V., Moreno, M., Ortega-Culaciati, F., Donoso, F., Báez, J. C., and Tassara, A. Mosaicking Andean morphostructure and seismic cycle crustal deformation patterns using GNSS velocities and machine learning. *Frontiers in Earth Science*, 11, Mar. 2023. doi: 10.3389/feart.2023.1096238.
- Zhang, Y., Zhang, G., Hetland, E. A., Shan, X., Wen, S., and Zuo, R. *Coseismic Fault Slip of the September 16, 2015 Mw 8.3 Illapel, Chile Earthquake Estimated from InSAR Data*, page 73–82. Springer International Publishing, 2017. doi: 10.1007/978-3-319-57822-4\_7.

The article *Application of Neural Networks for Estimating Coseismic Slip Distribution Using Synthetic GNSS Data* © 2025 by V. Inzunza is licensed under CC BY 4.0.